



## OPEN ACCESS

EDITED BY  
Jiabao Xu,  
University of Oxford,  
United Kingdom

REVIEWED BY  
Yi Wang,  
Southern University of Science and  
Technology, China  
Jing Zhang,  
Boston University,  
United States

\*CORRESPONDENCE  
Howbeer Muhamadali  
✉ howbeer.muhamad-ali@liverpool.ac.uk

SPECIALTY SECTION  
This article was submitted to  
Antimicrobials, Resistance and Chemotherapy,  
a section of the journal  
Frontiers in Microbiology

RECEIVED 22 October 2022  
ACCEPTED 12 January 2023  
PUBLISHED 01 February 2023

CITATION  
Shams S, Lima C, Xu Y, Ahmed S,  
Goodacre R and Muhamadali H (2023) Optical  
photothermal infrared spectroscopy: A novel  
solution for rapid identification of antimicrobial  
resistance at the single-cell level *via* deuterium  
isotope labeling.  
*Front. Microbiol.* 14:1077106.  
doi: 10.3389/fmicb.2023.1077106

COPYRIGHT  
© 2023 Shams, Lima, Xu, Ahmed, Goodacre  
and Muhamadali. This is an open-access article  
distributed under the terms of the [Creative  
Commons Attribution License \(CC BY\)](https://creativecommons.org/licenses/by/4.0/). The  
use, distribution or reproduction in other  
forums is permitted, provided the original  
author(s) and the copyright owner(s) are  
credited and that the original publication in this  
journal is cited, in accordance with accepted  
academic practice. No use, distribution or  
reproduction is permitted which does not  
comply with these terms.

# Optical photothermal infrared spectroscopy: A novel solution for rapid identification of antimicrobial resistance at the single-cell level *via* deuterium isotope labeling

Sahand Shams<sup>1</sup>, Cassio Lima<sup>1</sup>, Yun Xu<sup>1</sup>, Shwan Ahmed<sup>1,2</sup>,  
Royston Goodacre<sup>1</sup> and Howbeer Muhamadali<sup>1\*</sup>

<sup>1</sup>Centre for Metabolomics Research, Department of Biochemistry and Systems Biology, Institute of Systems, Molecular, and Integrative Biology, University of Liverpool, Liverpool, United Kingdom, <sup>2</sup>Department of Environment and Quality Control, Kurdistan Institution for Strategic Studies and Scientific Research, Sulaymaniyah, Kurdistan Region, Iraq

The rise and extensive spread of antimicrobial resistance (AMR) has become a growing concern, and a threat to the environment and human health globally. The majority of current AMR identification methods used in clinical setting are based on traditional microbiology culture-dependent techniques which are time-consuming or expensive to be implemented, thus appropriate antibiotic stewardship is provided retrospectively which means the first line of treatment is to hope that a broad-spectrum antibiotic works. Hence, culture-independent and single-cell technologies are needed to allow for rapid detection and identification of antimicrobial-resistant bacteria and to support a more targeted and effective antibiotic therapy preventing further development and spread of AMR. In this study, for the first time, a non-destructive phenotyping method of optical photothermal infrared (O-PTIR) spectroscopy, coupled with deuterium isotope probing (DIP) and multivariate statistical analysis was employed as a metabolic fingerprinting approach to detect AMR in Uropathogenic *Escherichia coli* (UPEC) at both single-cell and population levels. Principal component-discriminant function analysis (PC-DFA) of FT-IR and O-PTIR spectral data showed clear clustering patterns as a result of distinctive spectral shifts (C–D signature peaks) originating from deuterium incorporation into bacterial cells, allowing for rapid detection and classification of sensitive and resistant isolates at the single-cell level. Furthermore, the single-frequency images obtained using the C–D signature peak at 2,163cm<sup>-1</sup> clearly displayed the reduced ability of the trimethoprim-sensitive strain for incorporating deuterium when exposed to this antibiotic, compared to the untreated condition. Hence, the results of this study indicated that O-PTIR can be employed as an efficient tool for the rapid detection of AMR at the single-cell level.

## KEYWORDS

antimicrobial resistance, single-cell, microbiology, infrared spectroscopy, stable-isotope probing, Uropathogenic *Escherichia coli*

## 1. Introduction

Since the 1980s, due to the extreme and indiscreet consumption of antimicrobial agents in both humans and animals, antimicrobial resistance (AMR) has emerged (Boerlin and Reid-Smith, 2008; Sengupta et al., 2013), and become a worldwide threat. If actions are not taken to address this issue, it is estimated that by 2050 more than 10 million people will die annually from AMR alone, which is more than diabetes or cancer with 1.5 million and 8.2 million annual death cases, respectively (O'Neill, 2016).

Along with the increase in the number of resistant pathogens, AMR detection methodologies have also advanced (Charteris et al., 2001), and for clinical application, the development of quick antibiotic susceptibility testing (AST) has become a priority (Kerremans et al., 2008; van Belkum et al., 2019). If AST is realized, then judicious antimicrobials can be used, which also opens up the possibility of using old antibiotics for therapy and thus reserving new antibiotics for emergency cases. However, generally, manual AST approaches are exceedingly time-consuming and overshadowed by the level of expertise and errors of labor during the sample analysis (Reller et al., 2009). Thus, to carry out AST of pathogens against multiple antimicrobial agents at the same time, automated AST systems are largely being used to reduce labor and time requirements (Shanmugakani et al., 2020). The approved automated AST systems use various antimicrobial panels and technologies designed for testing the antimicrobial susceptibility of Gram-positive as well as Gram-negative pathogens (Reller et al., 2009). This is while, all commercially available instruments require up to 24 h to provide AST results (Shanmugakani et al., 2020).

During the past two decades, there has been a significant improvement in molecular and genotyping approaches for AMR detection, which has revolutionized the diagnosis of bacterial infections (Templeton, 1992; Anjum et al., 2017). Accompanied by the development of polymerase chain reaction (PCR) and its application, several forms of nucleic acid amplification tests (NAATs) including isothermal amplification were designed for the identification of AMR to one or multiple types of antimicrobials (Deiman et al., 2008; Ao and Jenison, 2013; Rivoarilala et al., 2018; Xu et al., 2018). Additionally, although whole-genome sequencing allows for a comprehensive understanding of resistance to entirely recognized antimicrobials as well as mechanisms (Köser et al., 2014; Oniciuc et al., 2018), compared to phenotypic tests such as enzymatic activity-based tests, bacterial growth-based tests and immunoassays, it is more expensive, requires significant infrastructure and is difficult to implement and needs a certain level of proficiency (Shanmugakani et al., 2020).

The utilization of single-cell technologies may lead to the development of rapid AST systems and the reduction of turnaround time, especially as there is the tantalizing possibility of making measurements without the need to culture the pathogen. Moreover, primary recognition of AMR in the microbial cells will be valuable to guide antimicrobial therapeutic strategies and preventing the progression of infection in the healthcare system (Bhattacharya, 2013; Simões et al., 2016).

Fourier transform infrared (FT-IR) spectroscopy is one of the most popular techniques by which the biochemical profile of biological samples, based on the vibrations of various IR-active biomolecules such as proteins, nucleic acids, carbohydrates and lipids, can be studied (Baker et al., 2014). As a whole-organism fingerprinting method, FT-IR spectroscopy has thrived to assess the progress of antibiotic resistance in bacteria (Salman et al., 2017; Sharaha et al., 2017). Previous studies

have also demonstrated the application of FT-IR spectroscopy for the detection and classification of bacterial cells at the population level (Muhamadali et al., 2016), the reader is directed to AlMasoud et al. (2021) for a recent review on the applications of whole-organism fingerprinting methods. The coupling of an FT-IR spectrophotometer to an optical microscope, on the other hand, provided a system that is capable of doing FT-IR microspectroscopy, which is a powerful tool that allows for the analysis of samples at small scale (e.g. particles with a diameter less than 150  $\mu\text{m}$ ; Nicosia and Stoops, 2017). However, FT-IR microspectroscopy provides a spatial resolution of 7–14  $\mu\text{m}$  and cannot distinguish structures smaller than a few micrometers due to the diffraction limit of the IR light, making it inefficient for imaging subcellular structures or single bacteria with dimensions typically ranging from 1 to 2  $\mu\text{m}$  (Bechtel et al., 2014). To address these drawbacks, Optical Photothermal Infrared (O-PTIR) spectroscopy, which is a novel far-field infrared imaging technique that works on the basis of the photothermal effects of infrared radiation, was developed. O-PTIR provides chemical images at submicron spatial resolution and evaluates the photothermal response of a sample irradiated by an adjustable mid-IR laser beam (Lima et al., 2021) in such a way that a pulsed tunable quantum cascade laser (QCL) IR laser is guided onto the sample surface and then, the IR source is made collinear with a 532 nm detection laser (green). The collinear beams are focused on the sample surface through a microscope objective. When the IR is absorbed by the sample, the thermal response of the sample surface is consequently monitored by the green detection laser. The reflected green light returns to the detector while the IR signal is extracted (Kansiz et al., 2020).

Previous studies employed mid-infrared imaging techniques for bacterial investigation, such as the study by Lima et al., which used O-PTIR spectroscopy combined with stable-isotope probing (SIP), in particular  $^{13}\text{C}$  and  $^{15}\text{N}$  isotopes, for imaging isotopically labeled bacteria at single-cell level. Such an approach allows for monitoring the molecular vibrations affected by the incorporation of “heavy” atoms into cellular biochemical components (Lima et al., 2021). Xu et al. (2020) also reported the application of Raman-integrated optical mid-infrared photothermal microscopy for detecting biochemical changes of bacteria in response to erythromycin within 1 h of exposure.

SIP can be defined as the use of stable (nonradioactive) isotopes that can act as a tracer and be used to monitor different biochemical activities in various biological systems. These stable isotopes, which include  $^2\text{H}$  (deuterium),  $^{13}\text{C}$ ,  $^{15}\text{N}$  and  $^{18}\text{O}$ , can be used during the growth phase of microorganisms so they can be incorporated into the structure of various biomolecules such as amino acids, fatty acids and nucleic acids (Muhamadali et al., 2015). In a previous study, we demonstrated the application of SIP, reverse SIP, and DIP combined with FT-IR and Raman spectroscopy, and secondary ion mass spectrometry (SIMS) for monitoring the metabolic activity of bacterial cells under various culturing conditions at the bulk level (Chisanga et al., 2021).

Previous studies have reported the use of deuterium oxide ( $\text{D}_2\text{O}$ ) combined with Raman microspectroscopy for the identification of active bacterial cells under specific growth conditions (Berry et al., 2015), to investigate cross feeding in microbial communities (Wang et al., 2016; Chisanga et al., 2021). Song et al. (2017) also reported the application of a similar strategy for the identification of bacteria resistant to carbenicillin and kanamycin, in samples isolated from the River Thames. However, to our best of knowledge so far, there are no studies in the literature reporting the combined application of DIP and O-PTIR spectroscopy for the detection of AMR at the single-cell level. Hence, in

this study, for the first time, we have employed FT-IR and O-PTIR spectroscopy combined with DIP, and multivariate statistical analysis techniques for the detection of AMR in Uropathogenic *Escherichia coli* (UPEC) isolates at both population and single-cell levels.

## 2. Materials and methods

### 2.1. Chemicals, microorganisms, and growth conditions

All chemical compounds used in this study were purchased from Sigma-Aldrich (United Kingdom) unless otherwise indicated. In addition to *E. coli* MG1655 which was used as the standard susceptible strain to trimethoprim (negative control), different UPEC isolates were selected from Dawson et al. (2014) and grown on Luria-Bertani (LB) agar from  $-80^{\circ}\text{C}$  glycerol stocks to obtain axenic colonies. Each isolate was subcultured 3 times on LB agar plates at  $37^{\circ}\text{C}$  overnight, before inoculating in LB broth. To culture the UPEC isolates in LB, colonies were chosen from the incubated agar plate and inoculated into 50 mL of fresh LB in 250 mL conical flasks and incubated at  $37^{\circ}\text{C}$  in a Brunswick G 25 shaker incubator (GMI, United States) at 180 rpm for 18 h.

### 2.2. Optimisation of D<sub>2</sub>O concentration

Following the procedure described in the growth conditions section, eight UPEC isolates were prepared and inoculated in fresh LB broth made with different concentration ratios of D<sub>2</sub>O/H<sub>2</sub>O ranging from 0 to 100% at intervals of 10%. The bacterial turbidity was adjusted to the standard optical density of 0.1 at 600 nm (OD<sub>600nm</sub>) and 200  $\mu\text{L}$  of these cultures was transferred to a sterile 100-well plate (3 biological replicates), followed by monitoring the bacterial growth profiles at OD<sub>600nm</sub> using a Bioscreen C spectrophotometer (Oy Growth Curves Ab Ltd., Finland). The following settings were used to run the instrument: preheating for 10 min, measurement intervals of 10 min, incubation temperature of  $37^{\circ}\text{C}$ , continuous medium shaking and 24 h of total experimentation.

### 2.3. Determination of trimethoprim minimum inhibitory concentration

In addition to *E. coli* MG1655, which was used as the standard strain for susceptibility testing to trimethoprim (TMP) with the minimal inhibitory concentration (MIC) value of 5 mg/L (Bhosle et al., 2020), all selected UPEC isolates were prepared following the procedure described in the growth conditions section. The prepared bacteria were then inoculated in fresh LB broth containing different concentrations of (5 mg/L, 7.5 mg/L and 10 mg/L), TMP and their growth profiles were recorded using the Bioscreen C, as described in the previous section.

### 2.4. Fourier transform infrared sample preparation and analysis

Following the incubation period and measurement of OD<sub>600nm</sub>, samples were centrifuged for 10 min at  $5,000\times g$  via a benchtop

Eppendorf centrifuge 5,910 R (Eppendorf Ltd., Cambridge, United Kingdom). The supernatant was removed and the biomass pellet was washed and resuspended 3 times using 1 mL of sterile physiological saline (0.9% NaCl) solution. The washed biomass was then stored at  $-80^{\circ}\text{C}$  until further analysis. In order to adjust for variation in the collected biomass, all samples were normalized by adjusting the bacterial turbidity to the OD<sub>600nm</sub> of 20. A total volume of 20  $\mu\text{L}$  of prepared cell suspension was then spotted onto a cleaned 96-well FT-IR silicon plate and heated in a  $55^{\circ}\text{C}$  oven until visibly dry ( $\sim 30$  min). FT-IR spectra were then acquired in absorbance mode using an INVENIO infrared spectrophotometer equipped with an HTS-XT high throughput plate reader (Bruker Optics Ltd., Coventry, United Kingdom). Each sample was averaged over 64 spectral scans, with integration time of 1 s per scan, between the  $4,000$  and  $400\text{ cm}^{-1}$  range with  $4\text{ cm}^{-1}$  resolution (Winder et al., 2006). The extended multiplicative signal correction (EMSC) method was then used to scale all obtained spectra (Afseth and Kohler, 2012), and CO<sub>2</sub> vibrations arising from the atmosphere ( $2,403$ – $2,272\text{ cm}^{-1}$ ) were eliminated from the spectra and replaced with a linear trend (Alsberg et al., 1998), prior to performing any multivariate statistical analysis.

### 2.5. Optical photothermal infrared analysis

A series of serial dilutions from the bacterial solutions were prepared in sterilized Milli-Q water to achieve the appropriate cell number and allow for dispersed cell deposition and chemical imaging at the single-cell level. All bacterial suspensions were also visually assessed using a light microscope, to ensure the integrity of the cellular membrane is not compromised. A total volume of 10  $\mu\text{L}$  of each concentration of samples was spotted on prewashed calcium fluoride (CaF<sub>2</sub>) slides, and air-dried in a desiccator. O-PTIR measurements were obtained from single bacterial cells on single-point mode, using a mIRage infrared microscope (Photothermal Spectroscopy Corp., Santa Barbara, United States). O-PTIR data ( $930$ – $1,800\text{ cm}^{-1}$  and  $1,970$ – $2,320\text{ cm}^{-1}$ ,  $2\text{ cm}^{-1}$  as spectral resolution, 10 scans per spectrum, with integration time of 10 s, and 3 spectra per bacterial cell) were collected in reflection mode through a Schwarzschild objective ( $40\times$ ,  $0.78\text{ NA}$ ); pump and probe beams consisting of a tunable QCL and a continuous-wave (CW) 532 nm laser, respectively (Lima et al., 2021, 2022). Single-frequency images were obtained by tuning the QCL to vibrational modes associated to amide I ( $1,655\text{ cm}^{-1}$ ) and C–D vibration ( $2,163\text{ cm}^{-1}$ ) at a 500 nm step size.

### 2.6. Data analysis

Once all the FT-IR and O-PTIR spectral data were collected, to remove spectra with low signal-to-noise ratio, all spectra with amide I signal intensities below 0.2 absorbance (arbitrary units) were excluded from further analysis. All data analyzes were carried out using MATLAB software version 2019a (MathWorks Inc., Natick, United States). The FT-IR and O-PTIR spectral data were then subjected to principal component analysis (PCA) to identify any natural clustering patterns. PCA is an unsupervised multivariate data analysis method, which is used to reduce the dimensionality of the data and as an exploratory data analysis tool. Its purpose is to extract important information from the data and to convert this information into a set of new orthogonal variables. PCA correspondingly signifies the pattern of similarity of the

observations and the variables by demonstrating them as points in maps (Abdi and Williams, 2010). This was then followed by principal component-discriminant function analysis (PC-DFA; Manly and Alberto, 2016). As a supervised discriminant technique, DFA minimizes the variance within a group of samples from the same class and maximizes the variance between samples from different classes. Based on the true representation of the principal components (PCs) of the sample of interest, this technique calculates distances between the centers of each PC for clustering purposes (Goodacre et al., 1998).

## 3. Results

### 3.1. Bacterial growth profile

The growth profiles of all UPEC isolates in this study were monitored in LB broth medium with varying concentration ratios of D<sub>2</sub>O/H<sub>2</sub>O, to identify the maximum concentration of D<sub>2</sub>O to be used in the DIP experiment, without having any visible negative side effects on the growth behavior of the bacteria. Based on the results achieved, 80% D<sub>2</sub>O was chosen as the optimal concentration, as it displayed minimal side effects on the growth phenotypes of the *E. coli* UTI isolates and MG1655, while also allowing for the detection of a reliable C–D vibration upon the IR analysis of the samples at single-cell level (Supplementary Figures S1A,B).

Following the optimisation of D<sub>2</sub>O concentration, the concentration of 5 mg/L of TMP was identified as the minimum inhibitory concentration (MIC), which is in agreement with the standards for assessing antibiotic susceptibility reported in the literature (Bhosle et al., 2020). To ensure that bacterial growth was inhibited efficiently, the concentration of 10 mg/L (2×MIC) was used in all the following experiments. According to the bacterial growth profiles (Supplementary Figures S1C,D), three susceptible (151, 122, and 147) and four resistant (6, 48, 123, and 143) isolates were identified; note that as expected *E. coli* MG1655 also showed no growth in the presence of TMP. Although at the initial first 6 h of the incubation period, a slight increase in OD<sub>600nm</sub> of some of the susceptible isolates was observed, however, the final biomass yield remained almost unchanged. All resistant isolates showed similar behavior in terms of growth rate and final biomass yield under both TMP-treated and untreated (control) conditions (Supplementary Figure S1C,D).

### 3.2. Fourier transform infrared spectroscopy at the population level

To investigate the quantitative capability of FT-IR spectroscopy combined with the DIP strategy for detection of deuterium incorporation, the standard *E. coli* MG1655 strain was incubated in LB broth medium with various concentration ratios of D<sub>2</sub>O/H<sub>2</sub>O, from 0–100% with 10% intervals. Looking at the FT-IR spectra of these samples (Supplementary Figure S2A), the C–D vibrations in the 2,500–2,000 cm<sup>-1</sup> region are clearly visible. These peaks appear due to the deuterium incorporation into bacterial cells, and hydrogen replacement, causing a change in the reduced mass ( $\mu$ ) (Muhamadali et al., 2015) of the corresponding vibrational bonds, resulting in the reduction of the naturally occurring C–H vibrational peaks (symmetric and asymmetric stretching vibrations of CH<sub>3</sub> and CH<sub>2</sub> functional groups) from the 3,000 to 2,800 cm<sup>-1</sup> wavenumber region to the new occurrence of C–D peaks at 2,500–2,000 cm<sup>-1</sup>. Upon zooming into this region, a clear linear trend is visible, showing an increase in the absorbance of the four main C–D

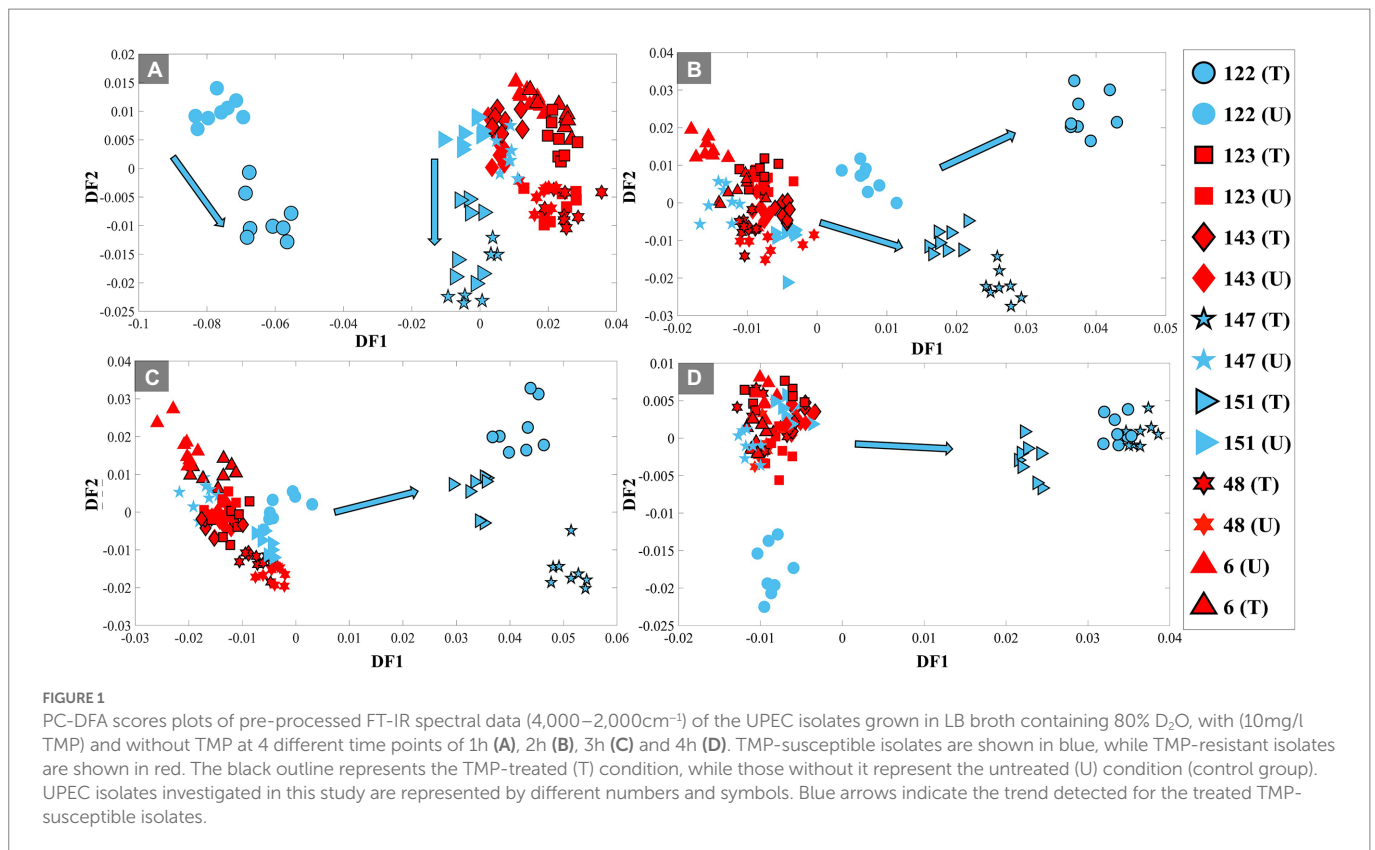
vibrations (2,471 cm<sup>-1</sup>, 2,418 cm<sup>-1</sup>, 2,195 cm<sup>-1</sup>, and 2,159 cm<sup>-1</sup>), corresponding directly to increasing D<sub>2</sub>O concentration in the medium from 0–100%. The PC-DFA scores plot of all the FT-IR spectral data, using the first 5 PCs accounting for 90.2% of the total explained variance (TEV), also displayed a clear D<sub>2</sub>O-dependent clustering pattern according to the DF1 axis, where samples with no D<sub>2</sub>O exposure were clustered on the far-left side of the axis, and samples with 100% D<sub>2</sub>O exposure were on the far positive side, and all other conditions were quantitatively clustered in between according to their D<sub>2</sub>O concentrations (Supplementary Figure S2B).

The loadings plot (Supplementary Figure S2C) showed the most significant vibrations that contributed to the observed clustering pattern, these include lipid bands (C–H and C–D) and protein bands (amide I and II), which allowed for the discrimination of bacterial groups grown in different concentrations of D<sub>2</sub>O. As it is demonstrated, the peaks at 2,925 cm<sup>-1</sup> and 2,854 cm<sup>-1</sup>, assigned to C–H stretching vibrations (Stuart, 1997), are in the negative part of DF1, while the peaks at 2,471 cm<sup>-1</sup> and 2,418 cm<sup>-1</sup> are on the positive side. This suggested that, as expected with increasing D<sub>2</sub>O concentration, the C–H bands' intensities decrease, while the C–D bands' intensities increase.

Next, all selected UPEC isolates were incubated in LB broth medium containing 80% D<sub>2</sub>O, with and without exposure to TMP, and samples were collected at four different time periods (1, 2, 3, and 4 h) for FT-IR (bulk) and O-PTIR (single-cell) analysis. The pre-processed FT-IR spectral data of all isolates, in addition to common vibrational peaks of bacterial cells (Table 1), displayed four additional peaks (C–D signature peaks) at the 2,500–2,000 cm<sup>-1</sup> wavenumber region, two of which, to our best of knowledge, are being reported for the first time using IR spectroscopy. As this study is aimed at using the C–D signatures for discriminating between TMP-sensitive and resistant isolates, in order to eliminate the contribution of the fingerprint region, subsequent analysis was mainly focused on the wavenumber region of vibrational peaks associated with deuterium incorporation (4,000–2,000 cm<sup>-1</sup>). Thus, all pre-processed FT-IR spectral data were combined and subjected to PC-DFA to identify any specific separation and clustering patterns resulting from the incorporation of deuterium. PC-DFA scores plots of the spectral data of all samples collected at 1 h timepoint at both conditions, TMP-treated and untreated, using 10 PCs accounting for 99.9% of the TEV (Figure 1A), showed slight discrimination between susceptible and resistant isolates according to DF1 axis. While both TMP-treated and untreated samples of the resistant isolates (123, 143, 48, and 6) displayed a tight cluster on the positive side of the DF2

TABLE 1 Common IR vibrational regions detected in bacteria, and their corresponding assignments (Stuart, 1997).

| Wavenumber (cm <sup>-1</sup> ) | Assignment                        | Nature of vibration           |
|--------------------------------|-----------------------------------|-------------------------------|
| 3,500–3,300                    | Proteins (Amide A)                | N–H stretching                |
| 3,000–2,800                    | Lipids                            | C–H stretching                |
| 2,500–2,000                    | Lipids                            | C–D stretching                |
| 1,730                          | Lipids                            | C=O stretching                |
| 1,700–1,600                    | Proteins (Amide I)                | C=O and C–N stretching        |
| 1,600–1,500                    | Proteins (Amide II)               | N–H bending; C–N stretching   |
| 1,350–1,250                    | Proteins (Amide III)              | C–N stretching; N–H bending   |
|                                |                                   | C=O stretching; O=C–N; Other  |
| 1,200–900                      | Nucleic acids and polysaccharides | P=O, C=O and C–O–C stretching |



axis, the TMP-treated samples of the sensitive isolates (122, 147, and 151) clustered on the negative side of DF2 axis, and the untreated samples were on the positive side. It is also perhaps worth noting that the DF1 axis is mainly dominated by the general biochemical differences between isolate 122 and the rest of the samples. Looking at the PC-DFA scores plots of the samples collected at subsequent timepoints (Figures 1B–D), it can be seen that the clustering patterns are starting to change from the 2h timepoint onwards, while resistant isolates remain to form a tight cluster for both TMP-treated and untreated cells, the TMP-treated sensitive isolates seem to move away from the untreated samples and starting to separate according to DF1 axis. This separation is even more evident at the 3 and 4h timepoints (Figures 1C,D), where the TMP-treated sensitive isolates are completely separated from the rest of the samples according to the DF1 axis. To explore other regions of the FT-IR spectral data, the full spectral range (4,000–400  $\text{cm}^{-1}$ ) as well as the “fingerprint” region (2,000–400  $\text{cm}^{-1}$ ) were also subjected to PC-DFA, following the same procedures mentioned above. Although the PC-DFA scores plots of these regions showed similar trend and clustering patterns, as expected, the degree of separation of TMP-treated groups of susceptible isolates from all other groups was not particularly evident until later timepoints (Supplementary Figures S3, S4).

Figure 2A illustrates the averaged ( $n=4$ ) FT-IR spectra of susceptible UPEC isolates, which clearly highlights the difference in the intensities of C–D vibrations at 2,471  $\text{cm}^{-1}$  and 2,418  $\text{cm}^{-1}$  upon exposure of these isolates to TMP. This is of course as expected, as the susceptible isolates could not incorporate  $\text{D}_2\text{O}$  when exposed to TMP, while the untreated cells were able to do so. Furthermore, the DF1 loadings plot (Figure 2B) of the FT-IR data at the 3h timepoint (Figure 1C), also confirmed that the most substantial peaks contributing to the discrimination of TMP-treated susceptible isolates from all other samples include: fatty acid vibrations at 2,925  $\text{cm}^{-1}$  and 2,854  $\text{cm}^{-1}$  which belong to the asymmetric and symmetric stretching vibrations of  $\text{CH}_2$ , respectively, and 2,471  $\text{cm}^{-1}$  and 2,418  $\text{cm}^{-1}$  which are

associated with the C–D stretching vibrations. These findings further indicate that the bacterial strains assessed in this study were mostly distinguished based on their ability to incorporate deuterium, and consequently showed a decrease in the intensity of C–H vibrational bands, while the intensities of C–D bands were increased. However, as expected, such metabolic activity is hindered in susceptible strains upon TMP treatment, hence significantly lower deuterium incorporation is detected.

### 3.3. Rapid trimethoprim antibiotic susceptibility testing for Uropathogenic *Escherichia coli* isolates using optical photothermal infrared spectroscopy at the single-cell level

To demonstrate the application of the DIP strategy combined with IR spectroscopy at single-cell level, susceptible (isolate No. 147) and resistant isolates (isolate No. 143) were selected from the tested UPEC collection, and assessed by O-PTIR spectroscopy. Single-cell O-PTIR measurements were carried out on focused sections of 10 individual single bacterial cells from each condition, including TMP-treated and untreated, of susceptible and resistant isolates. The collected O-PTIR spectra of UPEC isolates at single-cell level (Figure 3A; Supplementary Figure S5) showed significant similarities to FT-IR spectra at bulk level. The results also evidently showed the difference in the intensities of C–D vibrations at 2,195  $\text{cm}^{-1}$  and 2,159  $\text{cm}^{-1}$  as a result of TMP-exposure. Following the data processing described above, the 3D PCA scores plot of the O-PTIR spectral data at the 3h time point demonstrated a clear separation between the TMP-treated bacterial cells of the susceptible isolate from all other bacterial cells according to the PC1 axis with a TEV of 48.7% (Figure 3B). This is of course in agreement with the FT-IR findings (Figure 1), and as mentioned earlier

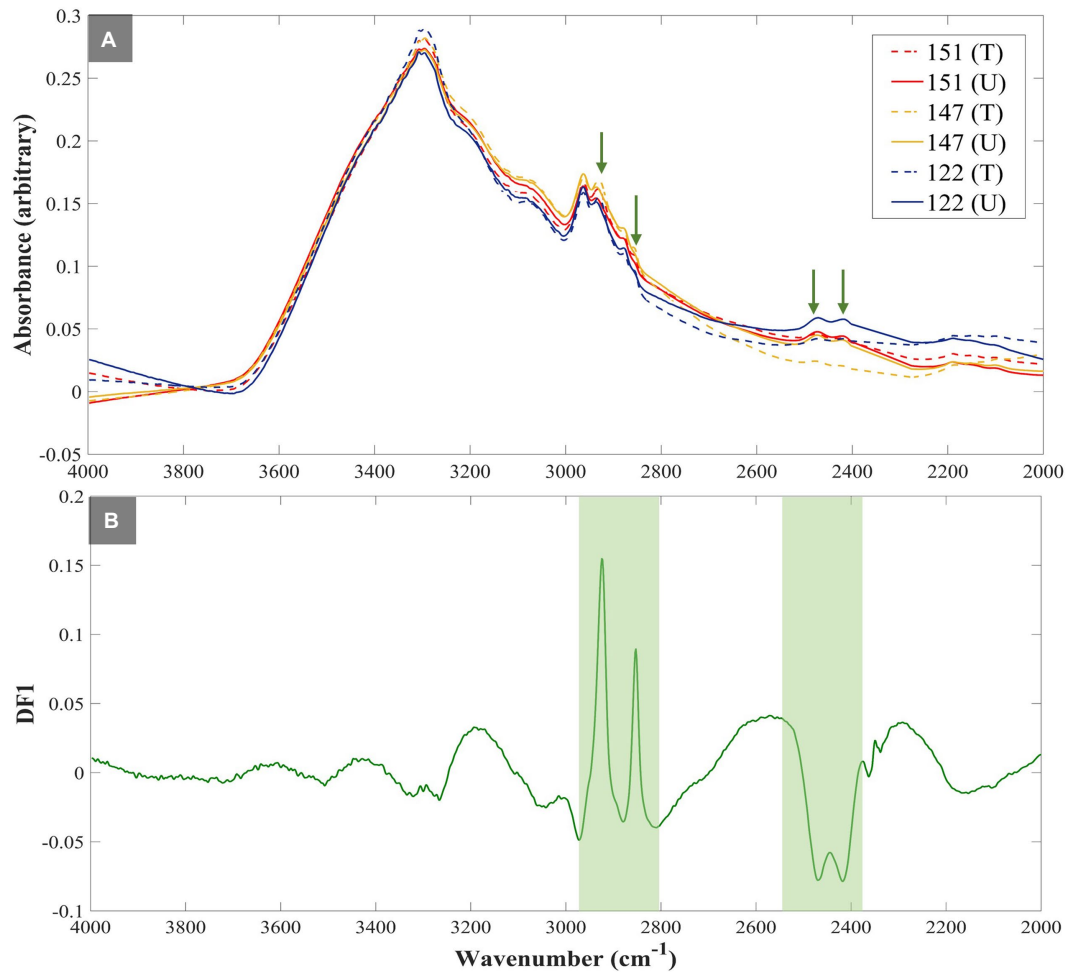


FIGURE 2

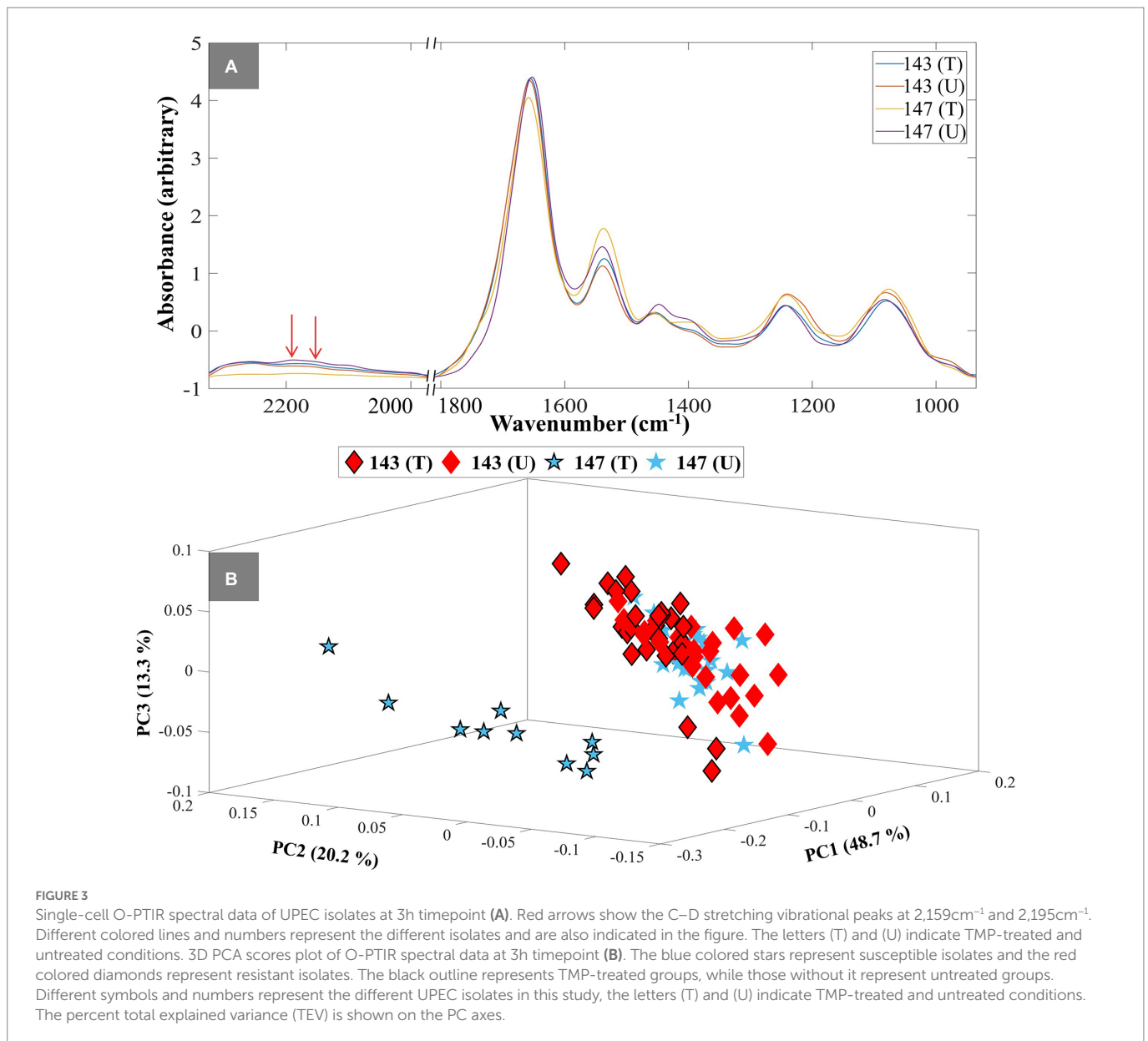
FT-IR spectra of susceptible UPEC isolates investigated in this study. The green arrows highlight the fatty acids'  $\text{CH}_2$  (at  $2,925\text{cm}^{-1}$  and  $2,854\text{cm}^{-1}$ ) and C–D stretching vibrations (at  $2,471\text{cm}^{-1}$  and  $2,418\text{cm}^{-1}$ ) (A), DF1 loadings plot of FT-IR spectral data at 3h timepoint illustrating the most significant vibrational peaks (green strips) contributing to the discrimination patterns (B). All spectra were normalized using extended multiplicative signal correction (EMSC). Each spectrum represents the average of four technical replicates. Different colored lines and numbers represent the different isolates, dotted lines represent treated groups, while untreated groups are represented as normal lines.

it is due to the inability of the susceptible isolate (147) to incorporate  $\text{D}_2\text{O}$  upon exposure to TMP, as they are not metabolically active, while other bacterial cells can continue to metabolise and incorporate deuterium. The 3D PCA scores plot of O-PTIR spectral data collected at the 4h timepoint also illustrated similar trends, where TMP-treated susceptible cells clustered separately from all other bacterial cells, according to the PC1 axis with TEV of 53.5% (data not shown). However, O-PTIR spectral data of bacterial cells collected at 1 and 2h timepoints did not display any distinct clustering for the susceptible and resistant isolates, as the C–D vibrations detected at these earlier timepoints were either below the detection limit of the O-PTIR instrument or unreliable, due to lower signal-to-noise ratio, at the single-cell level (data not shown). Hence, these data were not explored any further.

These findings highlight the sensitivity and reproducibility of O-PTIR for discrimination of susceptible and resistant bacterial strains. In order to explore the potential application of using only the C–D vibration for discrimination of resistant and sensitive isolates to TMP, the peak intensity of the C–D vibration at  $2,159\text{cm}^{-1}$  was normalized against the well-known amide I vibration at  $1,654\text{cm}^{-1}$ , and compared as box whisker plot (Figure 4). The results indicated that the TMP-treated bacterial cells of the susceptible isolate (147) had incorporated less deuterium in

comparison to the untreated bacterial cells from the same isolate (Figure 4). While according to the peak intensity ratio of the selected C–D band to amide I, the resistant isolate (143) incorporated almost the same amount of deuterium under both culturing conditions (Figure 4).

To demonstrate further the application of such a strategy for differentiating TMP-sensitive from resistant isolates at single-cell level, O-PTIR single-frequency images of the two *E. coli* isolates, TMP-susceptible (Figure 5) and resistant (Supplementary Figure S6), grown under both untreated and TMP-treated conditions were collected and compared by targeting the amide I and the C–D vibrational bands. Optical images of untreated (Figure 5A) and TMP-treated (Figure 5D) *E. coli* cells (isolate 147, TMP-susceptible) highlighted the position of individual cells. These bacterial cells grown under both untreated (Figure 5B) and TMP-treated (Figure 5E) conditions also displayed significant contrast from the background using the  $1,655\text{cm}^{-1}$  peak assigned to the amide I band of proteins. However, under the same field of view using the peak at  $2,163\text{cm}^{-1}$ , assigned to C–D vibration, while the untreated TMP-susceptible *E. coli* cells (Figure 5C) were clearly visible, suggesting that they are metabolically active and incorporating deuterium, the TMP-treated cells were hardly detected, suggesting that



they are not metabolically active and therefore, they could not incorporate deuterium (Figure 5F). This is while, both untreated (Supplementary Figure S6B) and treated (Supplementary Figure S6D) TMP-resistant *E. coli* cells (isolate 143) were clearly detected in the single-frequency images using both peaks at 1,655  $\text{cm}^{-1}$  and 2,163  $\text{cm}^{-1}$ , confirming the deuterium incorporation under both growth conditions.

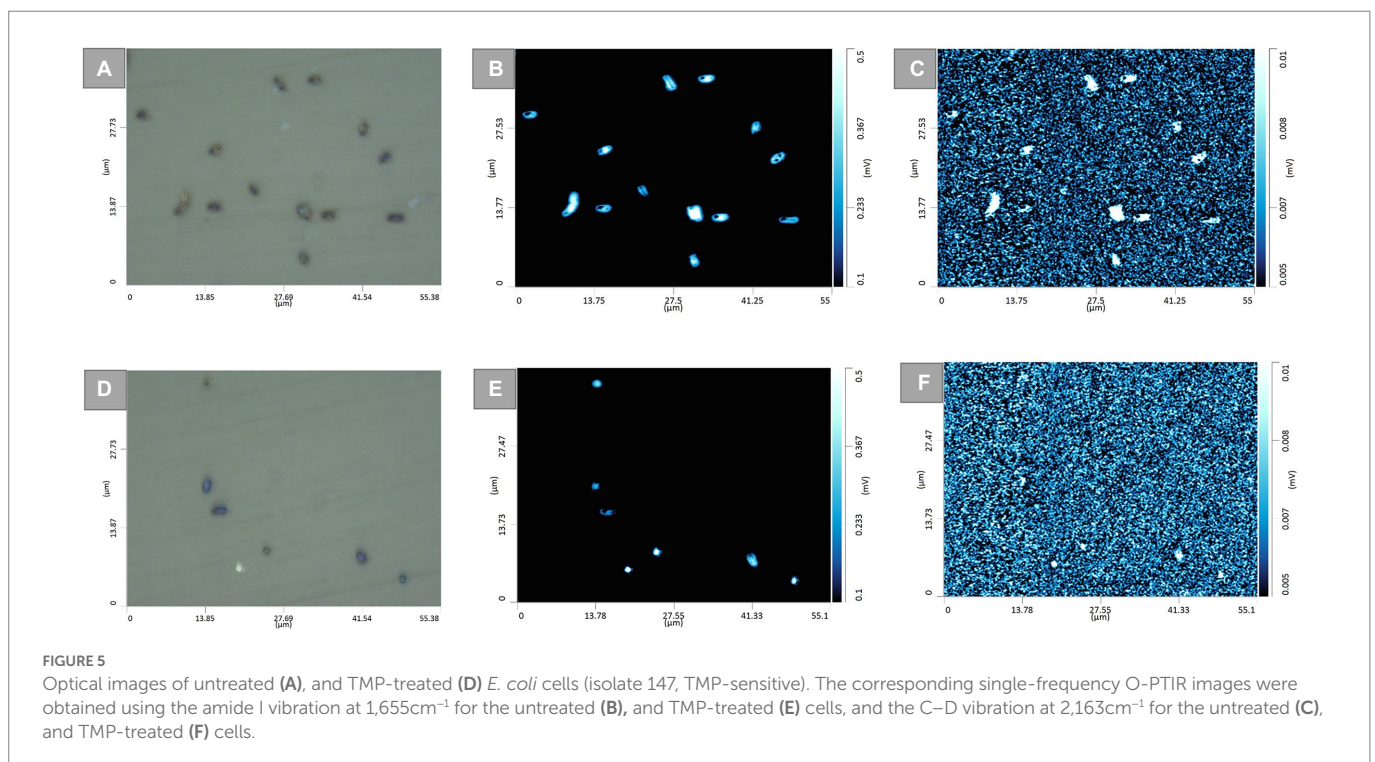
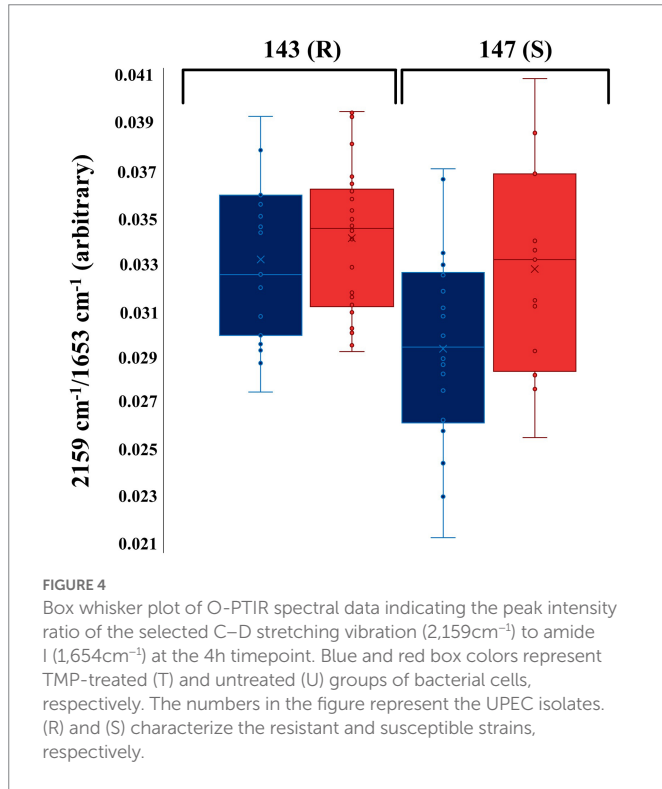
## 4. Discussion

There is no doubt that AMR has become one of the most pressing public health problems in the 21st century, threatening lives with a growing range of bacterial infections which in most cases no longer respond to commonly available medications and antibiotics (Prestinaci et al., 2015). Rapid recognition of antimicrobial-resistant bacteria accelerates the initiation of appropriate and targeted treatment and effective antibiotic therapy preventing further development and spread of AMR (Lery, 2002; Ellis et al., 2007; Marshall and Levy, 2011). During the past few decades,

stable-isotope labeling has been widely used to study microbial ecophysiology (Hernández et al., 2017), biogeochemical cycles (Radajewski et al., 2000), biotechnological procedures (Coyotzi et al., 2016) and human-disease interactions (Egert et al., 2007; Xu et al., 2021). This is because vibrational spectroscopic techniques (including infrared and Raman spectroscopies) have been employed for probing the cellular uptake of these stable isotopes and consequently detect chemical vibrations arising from the selective incorporation of isotopically labeled molecules (Haris et al., 1992; Berry and Loy, 2018). In spite of the extensive use of IR spectroscopy for AMR identification (Salman et al., 2017; Sharaha et al., 2017), the diffraction limit of the IR light has been the main barrier for acquiring IR chemical fingerprints at the submicron spatial resolution, especially when it comes to investigating individual bacterial cells (typically 1–2  $\mu\text{m}$ ). For this reason, research studies using IR spectroscopy were mostly conducted at the population level. This is while, in contrast to IR spectroscopy, Raman spectroscopy has proven to be an efficient fingerprinting tool for investigating samples at the single-cell level, as the diffraction limit provides an appropriate spatial resolution to study single cells (Bechtel et al., 2014).

To overcome the diffraction limitations, by employing continuous-wave visible lasers (532nm), O-PTIR measures the photothermal effect induced in IR-active samples by irradiating them with a tunable IR laser (Kansiz et al., 2020). Therefore, in this study, we aimed to explore the application of the DIP strategy combined with FT-IR and O-PTIR spectroscopy for the detection and discrimination of AMR in UPEC isolates at both population

and single-cell levels, respectively. The results of the FT-IR spectral data revealed that the corresponding intensities of a group of particular bands (C–D signature peaks; Supplementary Figure S2A) can be used for the discrimination of the susceptible and resistant bacteria to TMP. The PC-DFA scores plots of the spectral data collected at 1, 2, 3, and 4h timepoint (Figures 1A–D) indicated that the discrimination is not strain-dependent, and is instead due to the bacterial response to TMP treatment and its effect on the ability of the cells to undergo normal metabolism and thereby incorporate deuterium, which causes C–H vibrational bands that are generally assigned to fatty acids (but can of course be from any chemical that contains the C–H functional group) being shifted to the silent region (2,800–1,800  $\text{cm}^{-1}$ ; Naumann, 2000). The PC-DFA loadings plot (Figure 2B), also confirmed these findings as it displayed an increase in C–D vibration, upon incorporation of deuterium, while showing a decrease in the  $\text{CH}_2$  vibrations, suggesting that the investigated bacterial cells are metabolically active, meaning that the selected antibiotic does not affect the growth of those isolates, in other words the isolate is resistant to the selected antibiotic. It has been reported that lipids of both heterotrophic and autotrophic organisms contain a high proportion of water-derived protons (or  $\text{D}^+$  in the presence of  $\text{D}_2\text{O}$ ; Sessions et al., 2002; Valentine et al., 2004; Campbell et al., 2009; Zhang et al., 2009; Wegener et al., 2012) as during the reduction of NADP and NADH,  $\text{H}^+/\text{D}^+$  from  $\text{H}_2\text{O}/\text{D}_2\text{O}$  are transferred to these electron carries that are associated with cellular metabolic activity.  $\text{H}^+/\text{D}^+$  are then incorporated into lipids through fatty acid biosynthetic pathways forming C–D bonds (Sessions et al., 2002; Valentine et al., 2004; Zhang et al., 2009). In addition to lipids, D can also be incorporated into amino acids and carbohydrates through other biosynthetic pathways (Fischer et al., 2013; Justice et al., 2014). The results of the single-cell O-PTIR spectral data (Figure 3A; Supplementary Figure S5) displayed a significant resemblance to FT-IR showing efficacy of O-PTIR for identification of AMR. The PCA scores plot of the O-PTIR spectral data at the 3h timepoint (Figure 3B) successfully discriminated the TMP-treated bacterial cells of the susceptible isolate from all other bacterial cells. Also, the intensity ratio of the C–D





stretching vibration at  $2,159\text{ cm}^{-1}$  to amide I (Figure 4) in TMP-treated bacterial cells of the susceptible isolate was less than untreated bacterial cells of the susceptible isolate. This is while, this ratio was almost equal in both treated and untreated bacterial cells of the resistant isolate, emphasizing that these bacteria are resistant to the selected antibiotic, remain metabolically active and keep incorporating deuterium, highlighting the application of DIP strategy combined with IR spectroscopy for identification of AMR at single-cell level. In addition, in line with the single-cell O-PTIR spectral data, the O-PTIR single-frequency ( $2,163\text{ cm}^{-1}$ , assigned to C–D vibration) images of the TMP-susceptible bacterial cells grown in the presence of trimethoprim (Figure 5F), clearly displayed the significantly reduced ability of these cells to incorporate deuterium, compared to the cells grown under the untreated conditions (Figure 5C). This is while, the O-PTIR single-frequency images of the TMP-resistant bacterial cells' under both TMP-treated and untreated conditions (Supplementary Figures S6C,F) demonstrated distinct resemblance. It is also perhaps worth noting that some of the differences detected within the same bacterial community (Figure 4) could also be attributed to the high special resolution provided by the O-PTIR technology, which allows for the detection of such naturally occurring heterogeneity in the metabolic activity of the community at the single-cell level.

## 5. Conclusion and outlook

In this study for the first time, we report the employment of O-PTIR combined with deuterium isotope probing and multivariate statistical analysis, as an efficient tool for the AST of UPEC isolates at the single-cell level. The use of  $\text{D}_2\text{O}$  is particularly powerful as water is involved in many metabolic reactions and so the incorporation of deuterium into the cell will occur relatively quicker, while also being more cost effective, compared to the use of other stable isotopes such as  $^{13}\text{C}$  or  $^{15}\text{N}$ . According to our findings, the collected infrared spectra at bulk and single-cell levels showed substantial resemblances and reproducibility in the clustering pattern and were in complete agreement. FT-IR spectroscopy was also employed to demonstrate four C–D signature peaks ( $2,471\text{ cm}^{-1}$ ,  $2,418\text{ cm}^{-1}$ ,  $2,195\text{ cm}^{-1}$ , and  $2,159\text{ cm}^{-1}$ ), of which, to our best of knowledge, two of them ( $2,471\text{ cm}^{-1}$  and  $2,418\text{ cm}^{-1}$ ) are being reported here for the first time. However, unfortunately, these two vibrations were not detected at the single-cell level, as the spectral range of the O-PTIR instrument was limited to a specific range ( $2,320\text{--}1,970\text{ cm}^{-1}$  and  $1,800\text{--}930\text{ cm}^{-1}$ ), due to the restrictions in the maximum number of QCLs that can be used at any one time. To overcome this limitation, future studies can employ a tunable OPO-pulsed infrared laser to cover the higher wavenumber region of infrared radiation (Spadea et al., 2021). O-PTIR spectroscopy, individually or when combined with Raman spectroscopy such as the study conducted by Lima et al. (2022), can also be a powerful fingerprinting tool allowing scientists to gain novel insight into biological systems and bioprocesses of single bacterial cells. The results reported in this study successfully demonstrated that O-PTIR

spectroscopy can be employed as a promising tool for identifying AMR at the single-cell level.

## Data availability statement

The raw data supporting the conclusions of this article will be made available by the authors, without undue reservation.

## Author contributions

SS: experimental design, sample collection and preparation, FT-IR and O-PTIR data analysis, data interpretation, and manuscript writing. CL: sample preparation, O-PTIR data analysis and manuscript preparation. YX and SA: data analysis and interpretation. RG: experimental design, data interpretation, and manuscript preparation. HM: principal investigator, experimental design, sample collection and preparation, FT-IR and data analysis, data interpretation, and manuscript preparation. All authors contributed to the article and approved the submitted version.

## Acknowledgments

HM and RG would like to thank the University of Liverpool for funding and support.

## Conflict of interest

The authors declare that the research was conducted in the absence of any commercial or financial relationships that could be construed as a potential conflict of interest.

## Publisher's note

All claims expressed in this article are solely those of the authors and do not necessarily represent those of their affiliated organizations, or those of the publisher, the editors and the reviewers. Any product that may be evaluated in this article, or claim that may be made by its manufacturer, is not guaranteed or endorsed by the publisher.

## Supplementary material

The Supplementary material for this article can be found online at: <https://www.frontiersin.org/articles/10.3389/fmicb.2023.1077106/full#supplementary-material>

## References

- Abdi, H., and Williams, L. J. (2010). Principal component analysis. *Wiley Interdisciplin. Rev. 2*, 433–459. doi: 10.1002/wics.101
- Afseth, N. K., and Kohler, A. (2012). Extended multiplicative signal correction in vibrational spectroscopy, a tutorial. *Chemom. Intell. Lab. Syst.* 117, 92–99. doi: 10.1016/j.chemolab.2012.03.004
- AlMasoud, N., Muhamadali, H., Chisanga, M., AlRabiah, H., Lima, C. A., and Goodacre, R. (2021). Discrimination of bacteria using whole organism fingerprinting: the utility of modern physicochemical techniques for bacterial typing. *Analyst* 146, 770–788. doi: 10.1039/D0AN01482F
- Alsberg, B. K., Wade, W. G., and Goodacre, R. (1998). Chemometric analysis of diffuse reflectance-absorbance Fourier transform infrared spectra using rule induction methods: application to the classification of *Eubacterium* species. *Appl. Spectrosc.* 52, 823–832. doi: 10.1366/0003702981944562
- Anjum, M. F., Zankari, E., and Hasman, H. (2017). Molecular methods for detection of antimicrobial resistance. *Microbiol. Spectr.* 5:2017. doi: 10.1128/microbiolspec.ARBA-0011-2017
- Ao, W., and Jenison, R. (2013). "Detection of rpoB gene mutations using helicase-dependent amplification," in *Nucleic Acid Detection*. eds. D. M. Kolpashchikov and Y. V. Gerasimova (Totowa, NJ: Humana Press), 89–98.

- Baker, M. J., Trevisan, J., Bassan, P., Bhargava, R., Butler, H. J., Dorling, K. M., et al. (2014). Using Fourier transform IR spectroscopy to analyze biological materials. *Nat. Protoc.* 9, 1771–1791. doi: 10.1038/nprot.2014.110
- Bechtel, H. A., Muller, E. A., Olmon, R. L., Martin, M. C., and Raschke, M. B. (2014). Ultrabroadband infrared nanospectroscopic imaging. *Proc. Natl. Acad. Sci.* 111, 7191–7196. doi: 10.1073/pnas.1400521111
- Berry, D., and Loy, A. (2018). Stable-isotope probing of human and animal microbiome function. *Trends Microbiol.* 26, 999–1007. doi: 10.1016/j.tim.2018.06.004
- Berry, D., Mader, E., Lee, T. K., Woebken, D., Wang, Y., Zhu, D., et al. (2015). Tracking heavy water (D<sub>2</sub>O) incorporation for identifying and sorting active microbial cells. *Proc. Natl. Acad. Sci.* 112, E194–E203. doi: 10.1073/pnas.1420406112
- Bhattacharya, S. (2013). Early diagnosis of resistant pathogens: how can it improve antimicrobial treatment? *Virulence* 4, 172–184. doi: 10.4161/viru.23326
- Bhosle, A., Datey, A., Chandrasekharan, G., Singh, D., Chakravorty, D., and Chandra, N. (2020). A strategic target rescues trimethoprim sensitivity in *Escherichia coli*. *IScience* 23:100986. doi: 10.1016/j.isci.2020.100986
- Boerlin, P., and Reid-Smith, R. J. (2008). Antimicrobial resistance: its emergence and transmission. *Anim. Health Res. Rev.* 9, 115–126. doi: 10.1017/S146625230800159X
- Campbell, B. J., Li, C., Sessions, A. L., and Valentine, D. L. (2009). Hydrogen isotopic fractionation in lipid biosynthesis by H<sub>2</sub>-consuming *Desulfobacterium autotrophicum*. *Geochim. Cosmochim. Acta* 73, 2744–2757. doi: 10.1016/j.gca.2009.02.034
- Charteris, W. P., Kelly, P. M., Morelli, L., and Collins, J. K. (2001). Gradient diffusion antibiotic susceptibility testing of potentially probiotic *Lactobacilli*. *J. Food Prot.* 64, 2007–2014. doi: 10.4315/0362-028X-64.12.2007
- Chisanga, M., Muhamadali, H., McDougall, D., Xu, Y., Lockyer, N., and Goodacre, R. (2021). Metabolism in action: stable isotope probing using vibrational spectroscopy and SIMS reveals kinetic and metabolic flux of key substrates. *Analyst* 146, 1734–1746. doi: 10.1039/D0AN02319A
- Coytzi, S., Pratscher, J., Murrell, J. C., and Neufeld, J. D. (2016). Targeted metagenomics of active microbial populations with stable-isotope probing. *Curr. Opin. Biotechnol.* 41, 1–8. doi: 10.1016/j.copbio.2016.02.017
- Dawson, S., Gibreel, T., Nicolaou, N., AlRabiah, H., Xu, Y., Goodacre, R., et al. (2014). Implementation of Fourier transform infrared spectroscopy for the rapid typing of uropathogenic *Escherichia coli*. *Eur. J. Clin. Microbiol. Infect. Dis.* 33, 983–988. doi: 10.1007/s10096-013-2036-0
- Deiman, B., Jay, C., Zintilini, C., Vermeer, S., van Strijp, D., Venema, F., et al. (2008). Efficient amplification with NASBA<sup>®</sup> of hepatitis B virus, herpes simplex virus and methicillin resistant *Staphylococcus aureus* DNA. *J. Virol. Methods* 151, 283–293. doi: 10.1016/j.jviromet.2008.04.009
- Egert, M., De Graaf, A. A., Maathuis, A., De Waard, P., Plugge, C. M., Smidt, H., et al. (2007). Identification of glucose-fermenting bacteria present in an in vitro model of the human intestine by RNA-stable isotope probing. *FEMS Microbiol. Ecol.* 60, 126–135. doi: 10.1111/j.1574-6941.2007.00281.x
- Ellis, D. I., Dunn, W. B., Griffin, J. L., Allwood, J. W., and Goodacre, R. (2007). Metabolic fingerprinting as a diagnostic tool. *Pharmacogenomics* 8, 1243–1266. doi: 10.2217/14622416.8.9.1243
- Fischer, C. R., Bowen, B. P., Pan, C., Northen, T. R., and Banfield, J. F. (2013). Stable-isotope probing reveals that hydrogen isotope fractionation in proteins and lipids in a microbial community are different and species-specific. *ACS Chem. Biol.* 8, 1755–1763. doi: 10.1021/cb400210q
- Goodacre, R., Timmins, E. M., Burton, R., Kaderbhai, N., Woodward, A. M., Kell, D. B., et al. (1998). Rapid identification of urinary tract infection bacteria using hyperspectral whole-organism fingerprinting and artificial neural networks. *Microbiology* 144, 1157–1170. doi: 10.1099/00222787-144-5-1157
- Haris, P. I., Robillard, G. T., Van Dijk, A. A., and Chapman, D. (1992). Potential of carbon-13 and nitrogen-15 labeling for studying protein-protein interactions using Fourier-transform infrared spectroscopy. *Biochemistry* 31, 6279–6284. doi: 10.1021/bi00142a016
- Hernández, M., Neufeld, J. D., and Dumont, M. G. (2017). “Enhancing functional metagenomics of complex microbial communities using stable isotopes” in *Functional Metagenomics: Tools and Applications* (Berlin: Springer), 139–150.
- Justice, N. B., Li, Z., Wang, Y., Spaulding, S. E., Mosier, A. C., Hettich, R. L., et al. (2014). 15 N- and 2 H proteomic stable isotope probing links nitrogen flow to archaeal heterotrophic activity. *Environ. Microbiol.* 16, 3224–3237. doi: 10.1111/1462-2920.12488
- Kansiz, M., Prater, C., Dillon, E., Lo, M., Anderson, J., Marcott, C., et al. (2020). Optical photothermal infrared microspectroscopy with simultaneous Raman—a new non-contact failure analysis technique for identification of <10 μm organic contamination in the hard drive and other electronics industries. *Microscopy Today* 28, 26–36. doi: 10.1017/S1551929520000917
- Kerremans, J., Verboom, P., Stijnen, T., Hakkaart-van Roijen, L., Goessens, W., Verbrugh, H., et al. (2008). Rapid identification and antimicrobial susceptibility testing reduce antibiotic use and accelerate pathogen-directed antibiotic use. *J. Antimicrob. Chemother.* 61, 428–435. doi: 10.1093/jac/dkm497
- Köser, C. U., Ellington, M. J., and Peacock, S. J. (2014). Whole-genome sequencing to control antimicrobial resistance. *Trends Genet.* 30, 401–407. doi: 10.1016/j.tig.2014.07.003
- Lery, S. (2002). *How Misuse of Antibiotics Destroys Their Curative Powers, the Antibiotic Paradox*. Oxford: Oxford University Press.
- Lima, C., Ahmed, S., Xu, Y., Muhamadali, H., Parry, C., McGalliard, R. J., et al. (2022). Simultaneous Raman and infrared spectroscopy: a novel combination for studying bacterial infections at the single cell level. *Chem. Sci.* 13, 8171–8179. doi: 10.1039/D2SC02493D
- Lima, C., Muhamadali, H., Xu, Y., Kansiz, M., and Goodacre, R. (2021). Imaging isotopically labeled bacteria at the single-cell level using high-resolution optical infrared photothermal spectroscopy. *Anal. Chem.* 93, 3082–3088. doi: 10.1021/acs.analchem.0c03967
- Manly, B. F., and Alberto, J. A. N. (2016). *Multivariate Statistical Methods: A Primer*, Boca Raton, FL: Chapman and Hall/CRC.
- Marshall, B. M., and Levy, S. B. (2011). Food animals and antimicrobials: impacts on human health. *Clin. Microbiol. Rev.* 24, 718–733. doi: 10.1128/CMR.00002-11
- Muhamadali, H., Chisanga, M., Subaihi, A., and Goodacre, R. (2015). Combining Raman and FT-IR spectroscopy with quantitative isotopic labeling for differentiation of *E. coli* cells at community and single cell levels. *Anal. Chem.* 87, 4578–4586. doi: 10.1021/acs.analchem.5b00892
- Muhamadali, H., Subaihi, A., Mohammadtaheri, M., Xu, Y., Ellis, D. I., Ramanathan, R., et al. (2016). Rapid, accurate, and comparative differentiation of clinically and industrially relevant microorganisms via multiple vibrational spectroscopic fingerprinting. *Analyst* 141, 5127–5136. doi: 10.1039/C6AN00883F
- Naumann, D. (2000). “Infrared spectroscopy in microbiology,” in *Encyclopedia Analytical Chemistry*, Vol. 102 (Hoboken, NJ: John Wiley & Sons, Ltd), 131.
- Nicosia, C., and Stoops, G. (2017). *Archaeological Soil and Sediment Micromorphology*, Hoboken, NJ: John Wiley & Sons.
- O’Neill, J. (2016). *Tackling Drug-Resistant Infections Globally: Final Report and Recommendations. Review on Antimicrobial Resistance*. Wellcome Trust and HM Government.
- Oniciuc, E. A., Likotrafiti, E., Alvarez-Molina, A., Prieto, M., Santos, J. A., and Alvarez-Ordóñez, A. (2018). The present and future of whole genome sequencing (WGS) and whole metagenome sequencing (WMS) for surveillance of antimicrobial resistant microorganisms and antimicrobial resistance genes across the food chain. *Genes* 9:268. doi: 10.3390/genes9050268
- Prestinaci, F., Pezzotti, P., and Pantosti, A. (2015). Antimicrobial resistance: a global multifaceted phenomenon. *Pathogens Global Health* 109, 309–318. doi: 10.1179/2047773215Y.0000000030
- Radajewski, S., Ineson, P., Parekh, N. R., and Murrell, J. C. (2000). Stable-isotope probing as a tool in microbial ecology. *Nature* 403, 646–649. doi: 10.1038/35001054
- Reller, L. B., Weinstein, M., Jorgensen, J. H., and Ferraro, M. J. (2009). Antimicrobial susceptibility testing: a review of general principles and contemporary practices. *Clin. Infect. Dis.* 49, 1749–1755. doi: 10.1086/647952
- Rivoarilala, O. L., Garin, B., Andriamahery, F., and Collard, J. M. (2018). Rapid in vitro detection of CTX-M groups 1, 2, 8, 9 resistance genes by LAMP assays. *PLoS One* 13:e0200421. doi: 10.1371/journal.pone.0200421
- Salman, A., Sharaha, U., Rodriguez-Diaz, E., Shufan, E., Riesenberger, K., Bigio, I. J., et al. (2017). Detection of antibiotic resistant *Escherichia Coli* bacteria using infrared microscopy and advanced multivariate analysis. *Analyst* 142, 2136–2144. doi: 10.1039/C7AN00192D
- Sengupta, S., Chattopadhyay, M. K., and Grossart, H.-P. (2013). The multifaceted roles of antibiotics and antibiotic resistance in nature. *Front. Microbiol.* 4:47. doi: 10.3389/fmicb.2013.00047
- Sessions, A. L., Jahnke, L. L., Schimmelfmann, A., and Hayes, J. M. (2002). Hydrogen isotope fractionation in lipids of the methane-oxidizing bacterium *Methylococcus capsulatus*. *Geochim. Cosmochim. Acta* 66, 3955–3969. doi: 10.1016/S0016-7037(02)00981-X
- Shanmugakani, R. K., Srinivasan, B., Glesby, M. J., Westblade, L. F., Cárdenas, W. B., Raj, T., et al. (2020). Current state of the art in rapid diagnostics for antimicrobial resistance. *Lab Chip* 20, 2607–2625. doi: 10.1039/D0LC00034E
- Sharaha, U., Rodriguez-Diaz, E., Riesenberger, K., Bigio, I. J., Huleihel, M., and Salman, A. (2017). Using infrared spectroscopy and multivariate analysis to detect antibiotics’ resistant *Escherichia coli* bacteria. *Anal. Chem.* 89, 8782–8790. doi: 10.1021/acs.analchem.7b01025
- Simões, A. S., Couto, I., Toscano, C., Gonçalves, E., Póvoa, P., Viveiros, M., et al. (2016). Prevention and control of antimicrobial resistant healthcare-associated infections: the microbiology laboratory rocks! *Front. Microbiol.* 7:855. doi: 10.3389/fmicb.2016.00855
- Song, Y., Cui, L., López, J. Á. S., Xu, J., Zhu, Y.-G., Thompson, I. P., et al. (2017). Raman-deuterium isotope probing for in-situ identification of antimicrobial resistant bacteria in Thames River. *Sci. Rep.* 7, 1–10. doi: 10.1038/s41598-017-16898-x
- Spadea, A., Denbigh, J., Lawrence, M. J., Kansiz, M., and Gardner, P. (2021). Analysis of fixed and live single cells using optical photothermal infrared with concomitant Raman spectroscopy. *Anal. Chem.* 93, 3938–3950. doi: 10.1021/acs.analchem.0c04846
- Stuart, B. H. (1997). *Biological Applications of Infrared Spectroscopy*. Hoboken, NJ: John Wiley & Sons.
- Templeton, N. S. (1992). The polymerase chain reaction. History, methods, and applications. *Diagn. Mol. Pathol.* 1, 58–72. doi: 10.1097/00019606-199203000-00008
- Valentine, D., Sessions, A., Tyler, S., and Chidthaisong, A. (2004). Hydrogen isotope fractionation during H<sub>2</sub>/CO<sub>2</sub> acetogenesis: hydrogen utilization efficiency and the origin of lipid-bound hydrogen. *Geobiology* 2, 179–188. doi: 10.1111/j.1472-4677.2004.00030.x

- van Belkum, A., Bachmann, T. T., Lüdke, G., Lisby, J. G., Kahlmeter, G., Mohess, A., et al. (2019). Developmental roadmap for antimicrobial susceptibility testing systems. *Nat. Rev. Microbiol.* 17, 51–62. doi: 10.1038/s41579-018-0098-9
- Wang, Y., Song, Y., Tao, Y., Muhamadali, H., Goodacre, R., Zhou, N.-Y., et al. (2016). Reverse and multiple stable isotope probing to study bacterial metabolism and interactions at the single cell level. *Anal. Chem.* 88, 9443–9450. doi: 10.1021/acs.analchem.6b01602
- Wegener, G., Bausch, M., Holler, T., Thang, N. M., Prieto Mollar, X., Kellermann, M. Y., et al. (2012). Assessing sub-seafloor microbial activity by combined stable isotope probing with deuterated water and <sup>13</sup>C-bicarbonate. *Environ. Microbiol.* 14, 1517–1527. doi: 10.1111/j.1462-2920.2012.02739.x
- Winder, C. L., Gordon, S. V., Dale, J., Hewinson, R. G., and Goodacre, R. (2006). Metabolic fingerprints of *Mycobacterium bovis* cluster with molecular type: implications for genotype–phenotype links. *Microbiology* 152, 2757–2765. doi: 10.1099/mic.0.28986-0
- Xu, J., Li, X., Guo, Z., Huang, W. E., and Cheng, J.-X. (2020). Fingerprinting bacterial metabolic response to erythromycin by Raman-integrated mid-infrared photothermal microscopy. *Anal. Chem.* 92, 14459–14465. doi: 10.1021/acs.analchem.0c02489
- Xu, J., Wang, X., Yang, L., Kan, B., and Lu, X. (2018). Rapid detection of mcr-1 by recombinase polymerase amplification. *J. Med. Microbiol.* 67, 1682–1688. doi: 10.1099/jmm.0.000865
- Xu, J., Yu, T., Zois, C. E., Cheng, J.-X., Tang, Y., Harris, A. L., et al. (2021). Unveiling cancer metabolism through spontaneous and coherent raman spectroscopy and stable isotope probing. *Cancers* 13:1718. doi: 10.3390/cancers13071718
- Zhang, X., Gillespie, A. L., and Sessions, A. L. (2009). Large D/H variations in bacterial lipids reflect central metabolic pathways. *Proc. Natl. Acad. Sci.* 106, 12580–12586. doi: 10.1073/pnas.0903030106